OCEANOGRAPHY

Nutrient uptake plasticity in phytoplankton sustains future ocean net primary production

Eun Young Kwon[1,2]*, M. G. Sreeush[1,2]*, Axel Timmermann[1,2], David M. Karl[3], Matthew J. Church[4], Sun-Seon Lee[1,2], Ryohei Yamaguchi[5]

Annually, marine phytoplankton convert approximately 50 billion tons of dissolved inorganic carbon to particulate and dissolved organic carbon, a portion of which is exported to depth via the biological carbon pump. Despite its important roles in regulating atmospheric carbon dioxide via carbon sequestration and in sustaining marine ecosystems, model-projected future changes in marine net primary production are highly uncertain even in the sign of the change. Here, using an Earth system model, we show that frugal utilization of phosphorus by phytoplankton under phosphate-stressed conditions can overcompensate the previously projected 21st century declines due to ocean warming and enhanced stratification. Our results, which are supported by observations from the Hawaii Ocean Time-series program, suggest that nutrient uptake plasticity in the subtropical ocean plays a key role in sustaining phytoplankton productivity and carbon export production in a warmer world.

INTRODUCTION

Phytoplankton production removes dissolved inorganic carbon (C), nitrogen (N), and phosphorus (P) from ambient seawater and allocates these elements into cellular macromolecules such as C-rich carbohydrates and P-rich RNA (*1*, *2*). Approximately 10% of this newly synthesized phytoplankton production is exported out of the sunlit upper ocean into the interior of the ocean, constituting a globally substantial pathway for carbon sequestration over decadal to millennial time scales (*3*). Phytoplankton also form the base of marine food webs by supplying essential nutrients and energy to heterotrophs with far-reaching effects on fisheries and human food security (*4*). The elemental composition of phytoplankton, usually expressed as the molar ratios of C:N:P, is variable in time and space depending on taxa and environmental conditions such as nutrient availability and temperature (*1*, *2*, *5*–*12*). This plasticity of elemental allocations from molecules to communities is one of the key features that allows phytoplankton assemblages to acclimate and adapt to a wide range of environmental conditions (*13*–*15*). This stoichiometric plasticity adds considerable uncertainty to projections of marine net primary production (NPP) and the global carbon cycle, which depend, in part, on how phytoplankton C:N:P composition may respond to climate change (*16*) and how the stoichiometric modulation of NPP may feed back on rising atmospheric carbon dioxide (CO_2) (*17*, *18*).

Previous generations of Earth system models have projected significantly declining oceanic NPP in low latitudes where future surface warming and enhanced stratification lead to increased grazing pressure and reduced nutrient supply to the sunlit surface (*19*–*21*). The direct linkage of ocean warming, increased stratification, and decreased surface nutrients leading to an overall decline in ocean NPP was supported by multidecadal variations in surface chlorophyll concentrations and NPP in low latitudes, which were linked to observed changes in ocean stratification (*22*). However, despite the observed long-term trends of surface warming and stratification from the 1960s (*23*), no unequivocal long-term trend in oceanic NPP has been reported (*24*). In contrast, observations from the Hawaii Ocean Time-series (HOT) program in the North Pacific Subtropical Gyre reveal a positive trend in primary production over 1989–2019, especially within the lower portion (75 to 125 m) of the euphotic zone (*25*). This increase in primary production was sustained during the prolonged time period when surface concentrations of phosphate (PO_4) fell below a PO_4-stressed threshold of 0.05 to 0.06 μmol kg^{-1} (*25*, *26*), a low value even for the oligotrophic ocean (*27*).

The recent generation of Earth system models participating in Coupled Model Intercomparison Project Phase 6 (CMIP6) allows for greater physiological, taxonomical, and functional flexibility of phytoplankton and subsequent cycling of nutrients and carbon than previous generations (*28*–*31*). The increased complexity and flexibility have shifted future projections of marine NPP to an insignificant multimodel mean decline with a large uncertainty of up to ±20% (*28*). Other recent studies have also challenged the direct linkage between nutrient availability and NPP by suggesting that flexible elemental stoichiometry of phytoplankton can buffer the negative effects of warming on phytoplankton production (*13*, *17*, *18*) and organic carbon export (*15*). However, the buffering effects of phytoplankton stoichiometric plasticity on marine NPP and oceanic CO_2 uptake have been estimated to be small, with models of global NPP and export production differing by less than 5% in estimated declines from the 1990s to the 2090s between fixed and variable C:P assumptions (*17*, *18*). How phytoplankton C:P plasticity interplays with biogeochemical cycles to control global-scale marine NPP and carbon cycles remains uncertain.

Here, we hypothesize that phytoplankton C:P stoichiometric plasticity plays an important role in sustaining oligotrophic ocean NPP and export production during the 21st century. We will show observational support for the coupled changes in PO_4 availability,

[1]Center for Climate Physics, Institute for Basic Science, Busan 46241, South Korea. [2]Pusan National University, Busan 46241, South Korea. [3]Daniel K. Inouye Center for Microbial Oceanography: Research and Education, University of Hawai'i at Mānoa, Honolulu, HI 96822, USA. [4]Flathead Lake Biological Station, University of Montana, Polson, MT 59860, USA. [5]Japan Agency for Marine-Earth Science and Technology, Research Institute for Global Change, Yokosuka 237-0061, Japan.
*Corresponding author. Email: ekwon957@gmail.com (E.Y.K.); sreeushmg@pusan.ac.kr (M.G.S.)

phytoplankton elemental stoichiometry, and the upper ocean NPP and export production in the North Pacific Subtropical Gyre. Then, we explore the sensitivity of global ocean NPP and export production to PO_4 uptake plasticity using an Earth system model. The goal is to identify an important source of uncertainty in marine NPP projections and constrain 21st century ocean NPP changes through improved process understanding.

RESULTS

Observational support for ocean NPP sustainability

In situ measurements of the HOT program at Station ALOHA (A Long-term Oligotrophic Habitat Assessment) help constrain coupled changes in nutrient availability, phytoplankton elemental stoichiometry, and primary and export production over the past three decades. Our analyses of the ^{14}C-based measurements of primary production are consistent with the significantly increasing trend over 1989–2019, where the trend within the lower portion of the euphotic zone (a relative increase of 12.2 ± 5.6% per decade, where the ± range is an SE of the trend) is more pronounced than a trend within the upper portion (a relative increase of 5.0 ± 4.0% per decade) (fig. S1). The three-decade increase in ^{14}C-based primary productivity coincides with decadal-scale increases (1995–2019) in the abundance of *Prochlorococcus* and photosynthetic picoeukaryotes, two of the most abundant types of phytoplankton at Station ALOHA (fig. S1). In particular, the temporal variation of the picoeukaryote abundances within the lower portion of the euphotic zone is significantly correlated with that of the ^{14}C-based estimate of primary productivity with a correlation coefficient (r) of 0.45 ($P < 0.05$) when annual mean data are used without detrending. Although neither comprehensive nor sufficient, the phytoplankton data independently support decadal increases (or at least sustainability) in upper ocean productivity in this permanently oligotrophic region.

The concentrations of suspended particulate carbon (PC) and particulate phosphorus (PP) averaged over the top 125 m, comprising both living phytoplankton and nonliving materials, exhibit large temporal fluctuations over 1989–2019 (fig. S2). Unfortunately, assessing long-term trends in PP and its ratio with PC concentrations is not possible because of a modification in the PP analysis methods that began in November 2011. Nevertheless, the records show that the interdecadal variations in the C:P ratios of suspended particles are inversely correlated with the variations in ambient PO_4 concentrations [$r = -0.39$ ($P < 0.05$), when the monthly data are smoothed with a 12-month moving average] (Fig. 1A). In particular, the prolonged time period, 2002–2009, of anomalously low PO_4 concentrations coincides with a period when suspended particles were depleted in P relative to C (Fig. 1A and fig. S2). The overall sensitivity of a C:P ratio increase to a PO_4 decrease at Station ALOHA lies in between empirically derived hyperbolic and power-law relationships (*9*, *18*) based on global-scale spatial distributions of C:P ratios of suspended particles (*32*) and ambient concentrations of PO_4 (*33*) (Fig. 1, B and C). The dependence of C:P ratios on upper ocean averaged PO_4 concentrations also holds for sinking particles at 150 m (Fig. 1D) and is nearly identical for the upper and lower euphotic zone (fig. S3). The inverse relationship between the C:P ratios and PO_4 concentrations is also supported by the time-series data from the Bermuda Atlantic Time-series Study (BATS) located in the North Atlantic Subtropical Gyre (Fig. 1, B and D, and fig. S3) (*15*). These empirical relationships may reflect the large-scale responses in phytoplankton C:P ratios to PO_4 availability, integrating physiological and ecological responses such as P-sparing effect, including lower P storage, sulfur substitution of P in phospholipids, and phytoplankton community shifts (*9*, *11*, *15*, *18*).

Sensitivity experiments using an Earth system model

On the basis of the two observationally constrained relationships between phytoplankton C:P ratios and PO_4 concentrations (*9*, *18*), we explore the role of variable C:P in the sensitivity of the global carbon cycle to greenhouse warming using the Community Earth System Model version 2 (CESM2) (*34*, *35*). The model is run with historical radiative forcing from 1850 to 2014 and using the Shared Socioeconomic Pathway 3-7.0 (SSP3-7.0) for greenhouse gas emissions and land-use change pathway from 2015 to 2100 (*35*). The marine biogeochemistry module embedded in the CESM2 and its preceding versions have been shown that simulated oceanic nutrient cycles and primary production, and their interactions with climate variations are in good agreement with observational constraints (*26*, *36*–*38*). An important feature of the CESM2, relative to the models used previously to explore the role of flexible C:P in future carbon cycle changes (*17*, *18*), is a more realistic representation of marine nitrogen cycles with an explicit representation of N_2-fixing microbes (i.e., diazotrophs) that support new production (*36*, *37*, *39*). Bopp *et al.* (*30*) identified N_2 fixation as an important driver of future oceanic NPP responses to simulated 21st century climate changes. Our model simulations that include a prognostic representation of micronutrient iron (Fe) cycles (a primary limiting nutrient for N_2-fixing microbes) and flexible phytoplankton C:Fe ratios (*39*) highlight the importance of N_2 fixation and flexible C:Fe ratios in mediating the variable C:P effects on ocean NPP changes.

We performed three numerical experiments based on the following assumptions regarding phytoplankton C:P composition: (i) a globally uniform C:P ratio of 117 (*40*) (referred to as "fixed" experiment), (ii) variable C:P of a hyperbolic relationship with PO_4 (*9*) (referred to as "hyperbolic" experiment), and (iii) variable C:P dependency expressed as a power-law relationship with PO_4 (*18*) (referred to as "power-law" experiment). The C:N ratio of phytoplankton is fixed at 7.3 (*40*) in all experiments, resulting in a range of phytoplankton N:P ratios across the experiments depending on the variable C:P ratios. We assume that the simple empirical relationships hold for the 21st century changes in elemental compositions of all phytoplankton functional types (e.g., large and small phytoplankton and diazotrophs). Although this assumption needs to be verified with future field- and experiment-based studies, Moreno *et al.* (*41*) showed that a large-scale sensitivity of the global carbon cycle to P availability, generated by a physiological trait–based model considering multienvironmental factors, can be captured by a simple PO_4-based parametric model as long as the simple parameterization is constrained by currently available observations. Moreover, observational evidence (*7*) and culture experiments (*2*, *5*) support a critical role of nutrient supply in elemental allocations into phytoplankton cells and communities, justifying our assumption of PO_4 as a key driver of phytoplankton C:P plasticity. We consider the hyperbolic-based empirical relationship as the best approximation to the observed response of phytoplankton C:P ratios to PO_4 changes, given its proximity to the best fits to the time-series data (Fig. 1 and fig. S3). A comparison with the

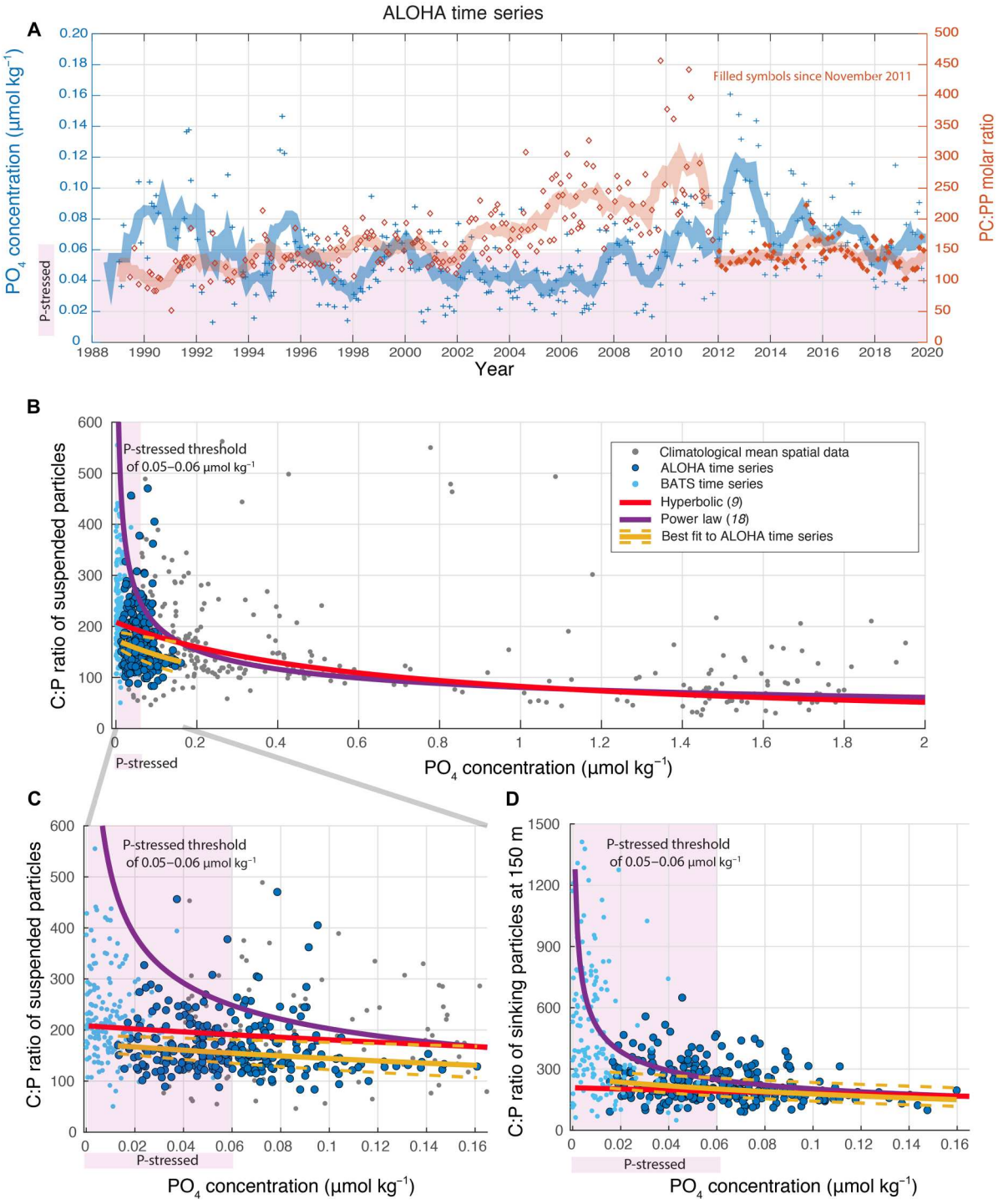

Fig. 1. Relationships between surface PO_4 and the C:P ratio of suspended and sinking particles. (**A**) Time series of monthly mean PO_4 concentrations (blue) and the ratio of PC concentration to PP concentration (red) averaged over depths of 0 to 125 m at Station ALOHA. The C:P ratios before November 2011 (a time of PP measurement method change) are shown as open diamonds, and those since November 2011 are shown as filled diamonds. Shaded red and blue lines are 12-month moving averages of the respective monthly mean data. The PO_4 concentrations lower than a P-stressed threshold of 0.06 µmol kg^{-1} (*26*) are shaded in purple. (**B**) Scatter plot showing the C:P ratios of suspended particles in the *y* axis and the surface PO_4 concentrations in the *x* axis. The ALOHA time-series data [presented in (A)] are shown in dark blue dots. The climatological mean spatially distributed data (gray dots) are taken from (*32*) and (*33*). The BATS time-series data are taken from (*15*) and plotted in sky blue dots. The two empirical relationships previously derived on the basis of the spatial data are shown as red [hyperbolic; Galbraith and Martiny (*9*)] and purple [power law; Tanioka and Matsumoto (*18*)] lines. The best fit to the ALOHA time-series data, P:C = (12.2 ± 7.4)‰ (per mil) × $[PO_4]$ + (5.8 ± 0.5)‰, is shown in yellow solid line with an SE denoted as yellow dashed lines. (**C**) Oligotrophic portion of (B) is zoomed in. (**D**) Scatter plot showing the C:P ratios of sinking particles at 150 m in the *y* axis and the surface PO_4 concentrations in the *x* axis. The best fit to the ALOHA time-series data is P:C = (17.2 ± 8.3)‰ × $[PO_4]$ + (3.9 ± 0.5)‰.

hypothetical case of the fixed phytoplankton C:P will allow us to explore the role of phytoplankton C:P plasticity in carbon cycles. We also use the power law–based empirical relationship, likely providing an upper bound of the C:P sensitivity to PO_4 depletion (*42*), as a measure of uncertainty for plausible future changes in phytoplankton C:P.

Ocean NPP sensitivity to phytoplankton C:P plasticity

The resulting projections of ocean NPP are highly sensitive to the phytoplankton C:P assumptions in oligotrophic regions. Consistent with most previous Earth system model projections (*19*, *20*, *28*), the simulations with a fixed C:P show a substantial future decline of a globally integrated ocean NPP by approximately 8% from 1850 to 2100 (Fig. 2A). The global-scale NPP reduction is mainly caused by declining NPP in oligotrophic gyres (Fig. 3F) covering ~40% of the global ocean surface area (oligotrophic gyres defined as the regions where the simulated present-day ocean surface PO_4 concentration is less than 0.2 mmol m^{-3}; Fig. 3C). This negative trend is partly offset by increases in NPP in the Southern Ocean and eastern equatorial Pacific Ocean (Fig. 3F). When we assume variable C:P, the globally integrated ocean NPP increases, reversing the sign of the NPP decline obtained from the fixed C:P case (Fig. 2A). The increasing NPP trends are dominated by increasing NPP in the Southern Ocean and eastern equatorial Pacific regions (Fig. 3H), where increasing light availability and temperature favor phytoplankton growth (*20*, *21*, *28*). On the other hand, NPP stays nearly unchanged from 1850 to 2100 in oligotrophic gyres relative to present-day conditions. The model simulates a negative NPP trend in the North Atlantic, which is more pronounced in the fixed C:P case (Fig. 3F) than the variable C:P case (Fig. 3H). The North Atlantic reductions in NPP occur in association with slowdown of the Atlantic meridional overturning circulation (*43*), which is also manifested in the CESM2 simulations presented here (*35*).

Hence, the stark contrast in the projected NPP changes between the fixed and variable C:P assumptions occurs in the oligotrophic gyres where the 2080–2100 averaged NPP is up to threefold larger in the variable C:P simulations than in the fixed C:P simulation (Fig. 4, A to C, and fig. S4). Within the low latitudes, enhanced ocean stratification leads to a large reduction in surface PO_4 availability in response to greenhouse warming (Figs. 3, A and D, and 5A). However, elevated phytoplankton C:P ratios under increasingly PO_4-stressed conditions overcompensate the nutrient stress effects on phytoplankton growth and NPP, as demonstrated in our decomposition analyses of the simulated differences between the variable and fixed C:P experiments (figs. S5 and S6). This compensation enables sustained phytoplankton growth rates and NPP in a warmer climate. The strengthened biological carbon pump under decreasing low-latitude surface PO_4 concentrations is qualitatively consistent with a previous study based on a box model (*9*).

The different treatment of phytoplankton C:P stoichiometry exerts a strong influence on P cycling in the ocean, which feeds back on the overall NPP responses to ocean warming driven PO_4 supply changes. Under the flexible C:P assumptions, the globally integrated PO_4 utilization rates are about ~70 Tg of P $year^{-1}$ (~9%) lower than those under the fixed C:P stoichiometry throughout the simulation period (Fig. 5C). The frugal utilization of PO_4 in the variable C:P case leads to a reduced organic P export out of the euphotic zone, elevating the PO_4 pool and retention time within the euphotic zone, relative to the fixed C:P case (Fig. 5, A, B, and E). Despite the reduced amount of organic P remineralized below the euphotic zone under the variable C:P assumptions, PO_4 stays elevated within the thermocline of the oligotrophic gyre (shallower than ~1000 m in depth) (Fig. 6) due to high preformed PO_4 subducted from the surface, which is, in turn, entrained and mixed back into the surface layers, fueling NPP. The increasingly frugal utilization of PO_4 with time decreases organic P production (equivalent to PO_4 uptake shown in Fig. 5C), which is decoupled with the time-invariant or slightly increasing organic C production rates under the variable C:P assumptions (Fig. 2A).

The leveraging effect of variable C:P on PO_4 availability is manifested as persistent N or combined N and Fe limitation on phytoplankton growth rates over time within most of the low-latitude

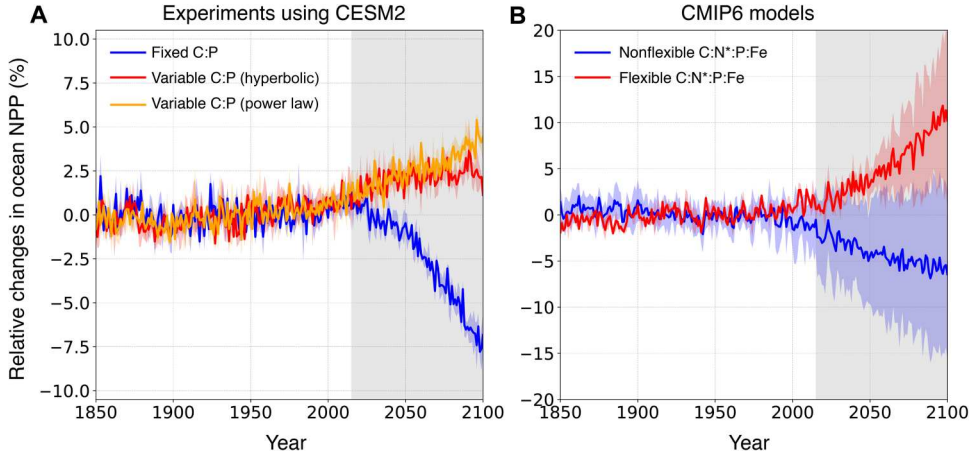

Fig. 2. Relative changes (with respect to 1850–2014 means) in the globally integrated ocean NPP with time. (**A**) Relative changes in NPP from the variable C:P experiment with an assumed hyperbolic relationship (red), the variable C:P experiment with an assumed power-law relationship (orange), and the fixed C:P experiment (blue). Solid line represents the average of three ensemble members for each experiment, and shade represents one SD. The projection period starting from 2015 is shaded in gray. (**B**) Relative changes in NPP from the CMIP6 models that allow flexible phytoplankton C:N*:P:Fe ratios (two models; table S1) are shown in red, with line denoting a multimodel average and shade denoting one SD. NPP changes from the models that do not allow flexible phytoplankton C:N*:P:Fe ratios (eight models; table S2) are shown in blue.

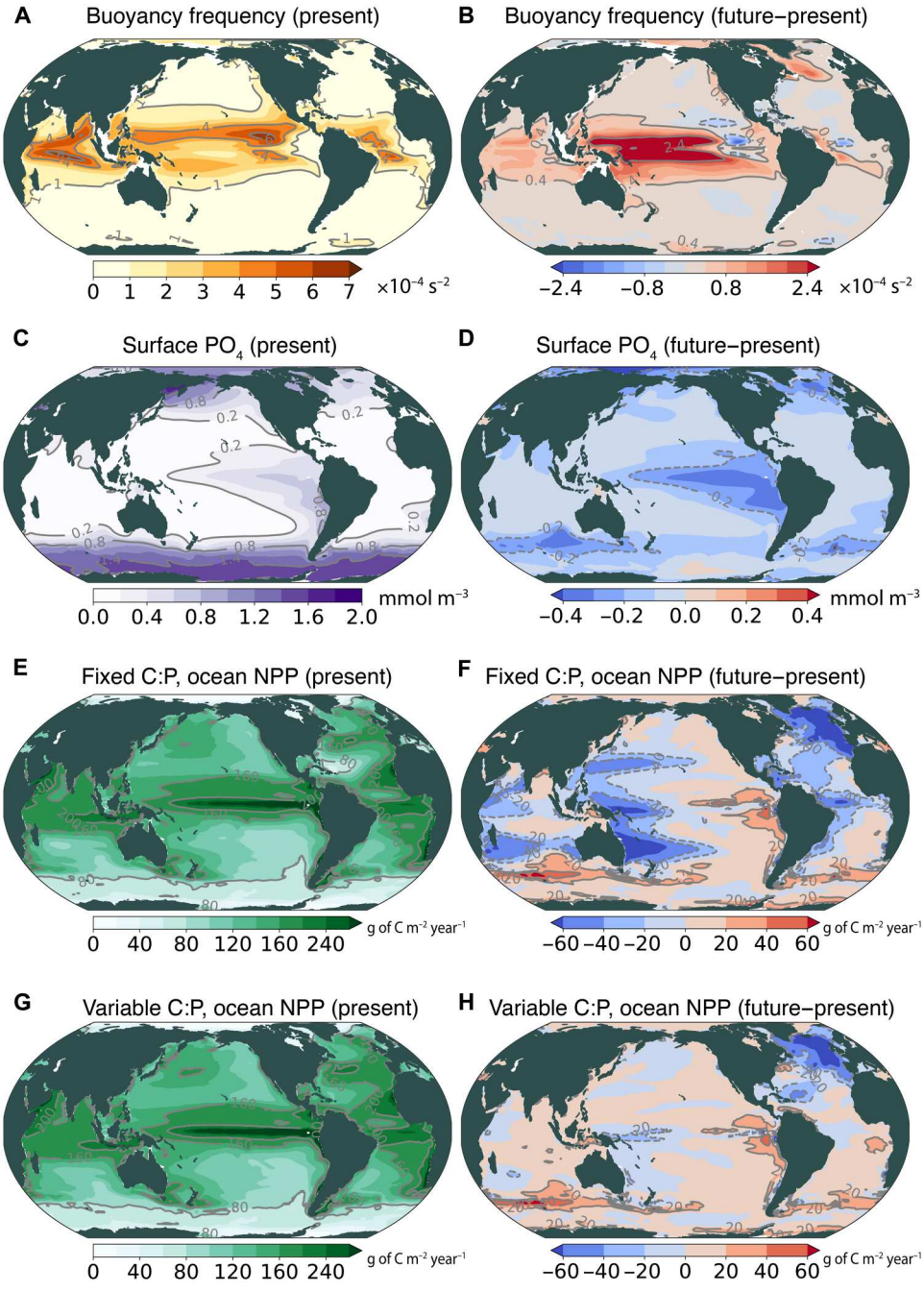

Fig. 3. Present-day means and future changes in ocean stratification, phosphate concentrations, and NPP. The panels on left column (A, C, E, G) show present-day means (1990–2010 average) and those on the right column (B, D, F, H) show future changes (2080–2100 average minus 1990–2010 average). (**A** and **B**) Buoyancy frequency (a measure of stratification) at 100 m. Buoyancy frequency is defined as $N^2 = -g/\rho_0 \cdot (\partial\rho/\partial z)$, where g is the acceleration of gravity, ρ_0 is a reference density, ρ is a local density, and z is the depth. Estimates from the fixed C:P experiment are shown. (**C** and **D**) Simulated surface PO_4 concentrations from the fixed C:P experiment. (**E** and **F**) Vertically integrated ocean NPP, simulated from the fixed C:P experiment. (**G** and **H**) Vertically integrated ocean NPP, simulated from the variable C:P experiment with a hyperbolic relationship between phytoplankton C:P and PO_4 concentrations.

surface ocean (figs. S7 and S8). Under fixed C:P stoichiometry, however, a higher P demand by phytoplankton quickly converts the low-latitude phytoplankton growth from N- or Fe-limited to P-limited and decreases ocean NPP in proportion to surface PO_4 decline (fig. S8). In the fixed C:P case, the PO_4-stress effect on the NPP decline dominates over the opposing effects from elevated utilization of dissolved organic phosphorus (DOP) by phytoplankton (Fig. 5D) and alleviated light limitation on growth rates (fig. S6). Relative to other limiting nutrients of N and Fe that are replenished by either N_2 fixation or aeolian deposition over large areas, a major external phosphorus source is limited to rivers, rendering the oceanic new production highly sensitive to P stress (*44*).

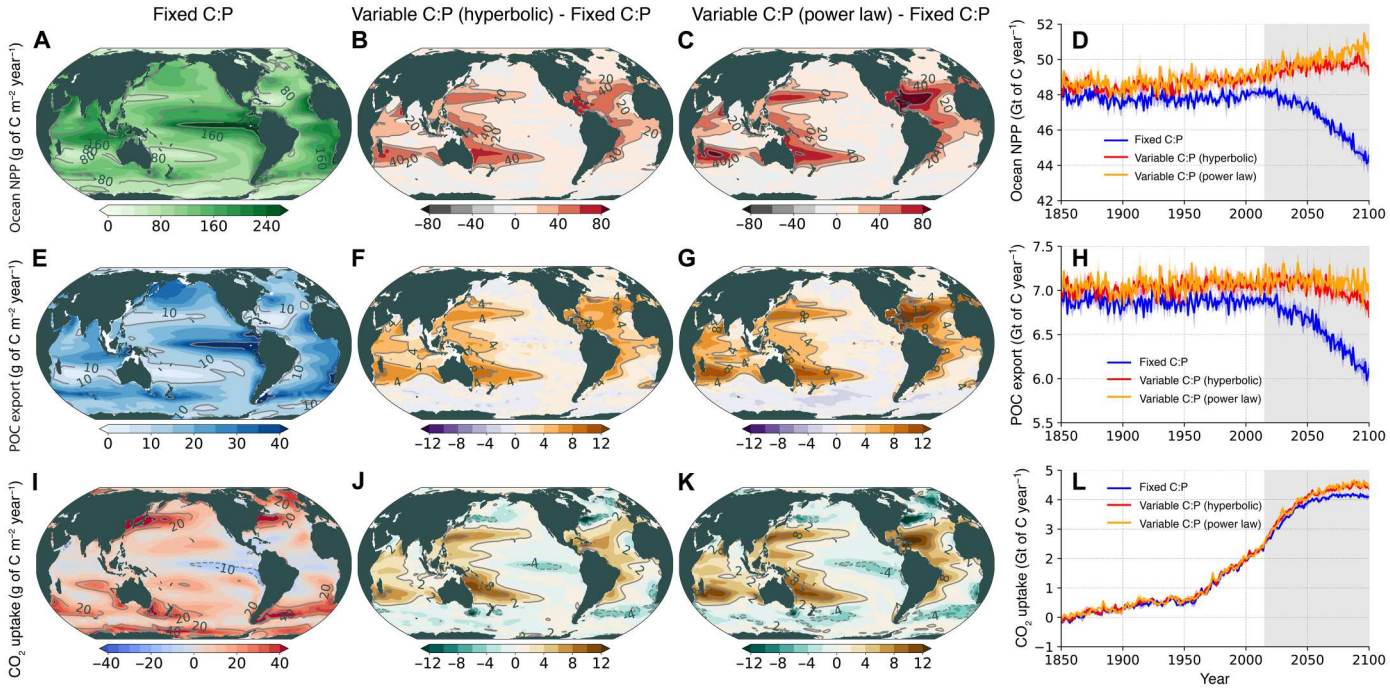

Fig. 4. Future projections (2080–2100 averages) from the fixed C:P experiment and differences between variable and fixed C:P experiments. (**A**) Future averaged, water column–integrated NPP, simulated from the fixed C:P experiment. (**B**) The NPP difference between the variable (hyperbolic) and fixed C:P experiments. (**C**) The NPP difference between the variable (power law) and fixed C:P experiments. (**D**) Globally integrated ocean NPP from three experiments. A three-member ensemble average is shown as solid line, and one SD is shown as shade. (**E** to **H**) Same as (A) to (D) except that the vertical export of particulate organic carbon (POC) at 100 m is shown. (**I** to **L**) Same as (A) to (D) except that the oceanic uptake of atmospheric CO_2 is shown. Positive values indicate fluxes into the ocean.

Sensitivity of POC export and CO_2 uptake

The stark contrast in NPP projections across the different C:P assumptions translates into substantial differences in vertical carbon export and oceanic CO_2 uptake toward the end of the 21st century (Fig. 4). While the globally integrated export production of particulate organic carbon (POC) decreases by ~0.9 Pg of C year^{-1} (~13%) from 1850 to 2100 under a fixed C:P assumption, it stays relatively constant over time under variable C:P assumptions (Fig. 4H). The muted increases in organic carbon export toward the end of the 21st century, despite global NPP increases in the variable C:P simulations, arise because of an increasing dominance of pico/nanophytoplankton in vast areas of low latitudes (fig. S9), sinking less efficiently to depths than large phytoplankton (*36*). The variable C:P effects are most pronounced in oligotrophic gyres where the projected organic carbon export at the end of this century differs by a factor of two relative to the carbon export with a fixed C:P (Fig. 4, E to G, and fig. S4). Greater removal rates of carbon from the sea surface, in turn, lead to greater uptake of CO_2 from the atmosphere. Regionally, the effect of variable C:P on CO_2 uptake amounts to more CO_2 uptake of up to 12 g of C m^{-2} year^{-1}, compared to the spatial range of an efflux of 20 g of C m^{-2} year^{-1} to an uptake of 50 g of C m^{-2} year^{-1}, as of 2080–2100 (Fig. 4, I to K). When globally integrated, however, the regionally enhanced uptake rates within the oligotrophic gyres are partly offset by reduced uptake or enhanced efflux rates within eutrophic regions, resulting in the enhancement of CO_2 uptake rates of approximately 0.4 Pg of C year^{-1} (10%) at the global scale. This result implies that variable phytoplankton C:P ratios could, in principle, act as negative feedbacks on rising atmospheric CO_2, although this feedback is not captured in the CESM2 simulations, because they ran with prescribed CO_2 concentrations rather than with a fully interactive carbon cycle. When globally averaged or integrated, the organic carbon export and air-sea CO_2 exchange inferred from the hyperbolic and power-law implementations of variable C:P are very similar. However, in strongly PO_4-stressed regions such as the North Atlantic Subtropical Gyre, the deviations from a fixed C:P assumption almost double when a power-law formulation is assumed (Fig. 4 and fig. S4). This large uncertainty on regional scales highlights the need for further refinement of the C:P relationships with environmental and ecological controls.

DISCUSSION

Consistent with previous studies (*17*, *18*), our results suggest that phytoplankton C:P plasticity can buffer the global warming effects on the 21st century ocean NPP and organic carbon export declines. This challenges the previous paradigm for understanding ocean NPP changes, i.e., surface warming and reduced surface nutrients directly leading to declining oceanic organic carbon production and export. Our results using the CESM2 show that the buffering effects are substantially larger than previously estimated (*17*, *18*), even reversing the sign of a global ocean NPP trend from negative to positive within the 21st century. Phytoplankton C:P plasticity synergistically interplays with N_2 fixation and C:Fe uptake plasticity in our model to sustain oligotrophic ocean NPP under a warmer climate. The synergistic effect of phytoplankton C:P plasticity on oligotrophic gyre NPP translates into substantial impacts on biological carbon export and oceanic uptake of

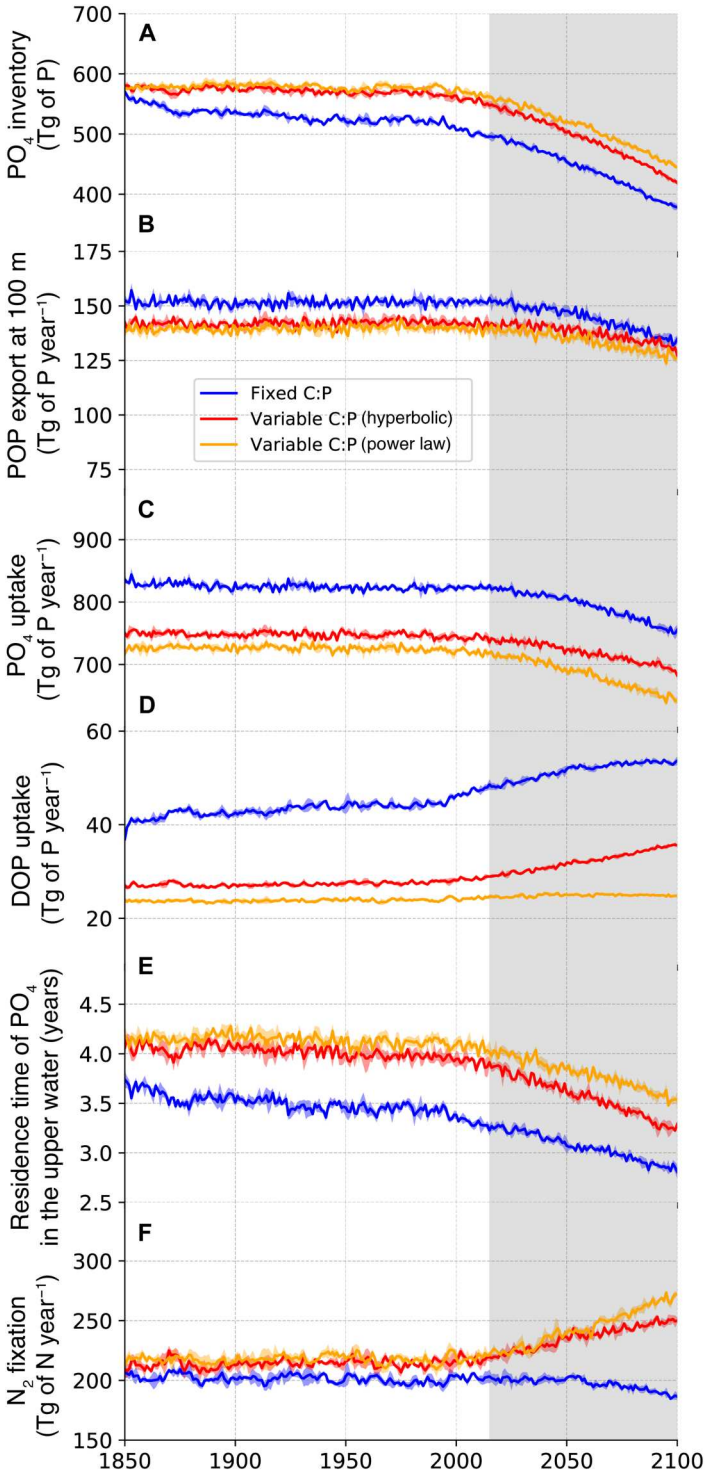

Fig. 5. Time series of model estimates from the three experiments The fixed C:P experiment (blue), the variable C:P experiment with a hyperbolic relationship between C:P and PO_4 (red), and the variable C:P with a power-law relationship (orange). (**A**) Globally integrated PO_4 inventory in the upper 100 m. (**B**) Globally integrated particulate organic phosphorus (POP) export at 100 m. (**C**) Globally integrated PO_4 uptake rates integrated over the top 100 m. (**D**) Globally integrated dissolved organic phosphorus (DOP) uptake rates integrated over the top 100 m. (**E**) Globally averaged retention time of PO_4 within the upper 100 m, as estimated by dividing the upper ocean PO_4 inventory with the POP export at 100 m. (**F**) Globally integrated N_2 fixation rates by phytoplankton. Solid line represents the average of three ensemble members for each experiment and shade represents one SD. A projection period of 2015–2100 is shaded in gray.

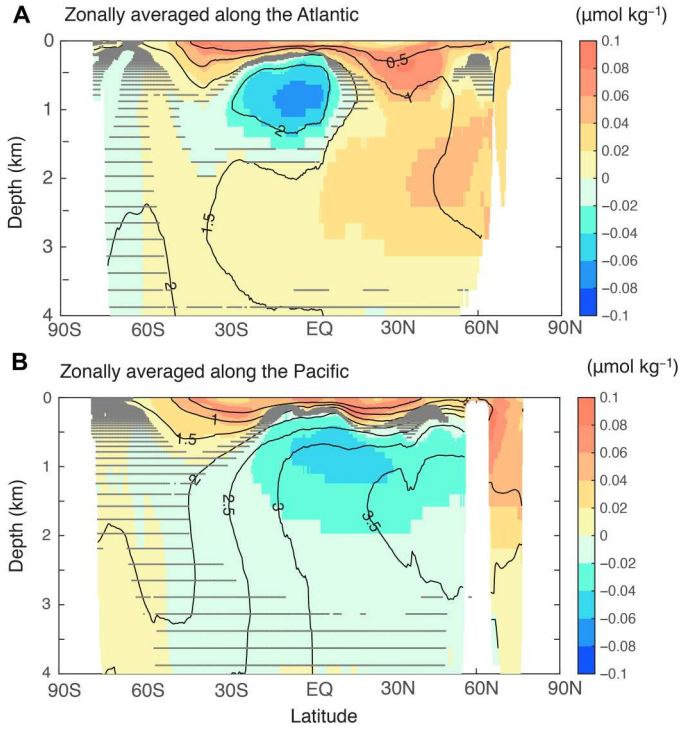

Fig. 6. Zonally averaged PO_4 difference between the variable and fixed C:P experiments, averaged over 2080–2100. The difference between the ensemble means from the variable (hyperbolic) and fixed C:P experiments is shown as shade, and the temporal mean over 2080–2100 of the variable (hyperbolic) experiment is shown as contour lines. The grid cells where the PO_4 difference does not exceed an SD across the ensemble members (indicating insignificant values with a 68% confidence interval) are marked with gray dots or stripes. (**A**) Zonally averaged along the Atlantic Ocean. (**B**) Zonally averaged along the Pacific Ocean.

atmospheric CO_2. The tight coupling between nutrient uptake plasticity and nutrient cycles and their interactive feedbacks on ocean NPP highlight the need for consideration of the biogeochemical interactions when assessing future changes in phytoplankton stoichiometric ratios and marine organic carbon production and export.

Our model-based sensitivity experiments, motivated by the observational constraint at Station ALOHA, can, in turn, provide insights into potential drivers for the observed decadal sustainability of ocean NPP in the North Pacific Subtropical Gyre. Direct linkages between our model results and the three decades of measurements at Station ALOHA are, however, challenging because of the model's simple representations of phytoplankton sources/sinks (e.g., lumping photosynthetic cyanobacteria and pico/nanophytoplankton as a single phytoplankton functional type of small phytoplankton) and because of different metrics used for comparison (i.e., simulated NPP versus ^{14}C-based primary productivity). Nevertheless, the increasing primary production observed at Station ALOHA over the past three decades is, at least, qualitatively consistent with the projected oligotrophic gyre NPP sustainability under the variable C:P assumption. In our model, the oligotrophic gyre NPP is sustained mainly because of elevated growth rates and biomass of a dominant phytoplankton functional type (i.e., small phytoplankton) under the variable C:P case relative to the fixed C:P case (fig. S8), which is in accordance with the observed increases in the abundance of dominant phytoplankton types at Station ALOHA. The small phytoplankton community outcompetes the large phytoplankton community in oligotrophic regions and takes advantage of stoichiometric plasticity when nutrients are depleted. The larger phytoplankton community becomes more competitive at the periphery of the oligotrophic regions when the C:P plasticity is permitted (fig. S10), contributing to the net NPP and carbon export increases in those regions.

Although the contribution is ~6% of the oligotrophic ocean NPP, N_2-fixing microbes also contribute to the 21st century NPP sustainability under flexible C:P assumptions (figs. S5, S6, and S8 to S10). As a result, more nitrogen is introduced from the atmosphere to the ocean's surface, meeting the elevated phytoplankton N:P requirements under the variable C:P assumption (Fig. 5F). The external source of N mediates the flexible C:P effect on sustaining future ocean NPP through an increased N availability within the euphotic zone, thereby explaining the greater simulated impacts of phytoplankton C:P plasticity on global ocean NPP obtained in our study, as compared to previous studies (*17*, *18*, *30*). The coupled changes in C:P ratios and N_2 fixation also explain the disproportionately higher sensitivity of ocean NPP to phytoplankton C:P plasticity in the warm subtropical gyre [where bottom-up nutrient, light, and temperature controls and top-down grazing pressure by zooplankton favor both diazotroph growth and biomass (*37*)]. Increases in suspended particulate organic matter (POM) N:P and C:P ratios observed at Station ALOHA between 1989 and 2005 have been attributed to stimulation of N_2 fixation by residual PO_4 in the near-surface ocean (*45*). N_2-fixing microbes have been considered as important members of the primary producer community in these oligotrophic regions (*37*, *46*, *47*) due to regular supplies of dissolved Fe through oceanic mesoscale eddies and atmospheric depositions (*26*, *48*). On the basis of the analogy between our model and the observations, we suggest that nutrient uptake plasticity in phytoplankton is a key to understand the 21st century changes in ocean NPP at Station ALOHA. Combined with a previous study (*15*) that suggested important roles of phytoplankton C:P composition and upper ocean P recycling in sustaining POC export in the North Atlantic Subtropical Gyre, we infer that the regulatory role of phytoplankton C:P plasticity in organic carbon production and export may be a unanimous feature for oligotrophic regions in general.

Our results identify an important cause for the wide range of future marine NPP projections among the models participating in CMIP6. A group of Earth system models that implement flexible phytoplankton C:P composition along with prognostic representations of N_2 fixation or flexible phytoplankton C:N ratios (referred to as flexible C:N*:P:Fe hereinafter, where N* is a measure of excess N uptake relative to C or P uptake by phytoplankton beyond a fixed ratio of C:N:P) (table S1) projects globally increasing NPP as the ocean warms and becomes more stratified (Fig. 2B and fig. S11A). On the other hand, the rest of the Earth system models (table S2) tend to project overall declining marine NPP with two exceptions that use the same ocean biogeochemistry module: Projected NPP increases in those models result from alleviating P stress by releasing additional PO_4 during N_2 fixation (mimicking an unresolved utilization of DOP pool by diazotrophs) (*30*), conceptually consistent with a critical role of upper ocean P availability in NPP sustainability advocated in our study. The 21st century projections of POC export out of the euphotic zone also remain distinct between the

two groups of Earth system models, with the models of flexible C:N*:P:Fe tending to project less reduction in the biological carbon export (fig. S11B). We note that substantial portions of projection uncertainties remain unexplained by different C:N*:P:Fe assumptions, partly because of varying degrees of warming-induced autotrophic and heterotrophic controls on ocean NPP and export production that are poorly constrained (*20*, *43*).

Apparently, phytoplankton have adopted biochemical and physiological strategies to cope with changing physical and chemical properties, which have evolved over millions of years of Earth's history (*14*). While we show here that, under limiting concentrations, the bulk cellular C:P ratio may increase, an alternate strategy for survival in P-stressed systems might be to take up extra P, in excess of that needed for growth and reproduction, and to store it as polyphosphates for subsequent use during periods of P scarcity (*49*). A previous study (*46*) also argued that some phytoplankton, especially N_2-fixing microbes, can acquire P by vertically migrating to P-replete subsurface waters. These physiological processes, as well as the interactive temperature and nutrient-supply control of phytoplankton C:P, may evolve in ways that are not necessarily consistent with the assumed contemporary relationship between surface PO_4 concentrations and phytoplankton C:P uptake, likely generating additional uncertainty (*10*, *12*, *16*) beyond those discussed here. Additional sources of uncertainty include an assumption of the C:P responses that are equally applied to all phytoplankton functional types and an assumption of a fixed phytoplankton C:N, all of which could lead to an uncertainty in relative contributions of each phytoplankton function type to the simulated NPP responses. How marine heterotrophs and food webs would respond to changing phytoplankton C:P ratios and how they may feed back on nutrient cycling also remain highly uncertain (*10*, *15*). Future Earth system models will need to include more mechanistically and observationally based parameterizations for phytoplankton nutrient uptake plasticity and subsequent cycling of the elements as the stoichiometric plasticity holds the key to a more realistic projection of future changes in climate–marine life interactions.

MATERIALS AND METHODS

ALOHA data analyses

The HOT data provide the best observational records for the study of upper ocean P cycles and primary production changes over the past three decades, due to its unprecedented long-term, continuous monitoring of P content in seawater and suspended/sinking particles (*25*, *50*, *51*). Station ALOHA is located in the North Pacific Subtropical Gyre at 22°45′N, 158°W (*52*). We used the time-series data of water-column PO_4 concentrations, suspended/sinking PC and PP, ^{14}C-based primary productivity, and the abundance of phytoplankton taxa or types (*Prochlorococcus*, *Synechococcus*, and picoeukaryotes), available at https://hahana.soest.hawaii.edu/hot/hot-dogs/interface.html. We used phosphate [termed as "low-level phosphorus" in the archive and also termed as soluble reactive phosphorus in literature (*15*, *25*)] measurements based on a high-sensitivity magnesium-induced coprecipitation (MAGIC), which has a detection limit of ~0.005 μmol kg^{-1} and is preferred for the study of the oligotrophic ocean (*15*, *26*, *27*). The use of PO_4 measurements based on an autoanalyzer does not change our conclusions, because the interdecadal PO_4 variations are similar between the two different methods (fig. S2). The suspended and sinking particles include both organic and inorganic matter, the latter of which is negligible for suspended matter and constitutes 10.4 ± 4.6% of sinking carbon (*25*). We refer readers to the previous studies (*25*, *50*, *51*) for detailed descriptions of data sampling and measurements.

The ALOHA time-series data have been mostly sampled at discrete depths of 5, 25, 45, 75, 100, and 125 m at near-monthly intervals. For an objective mapping, we grouped the data according to their sampling depths and time. We discretized the depth-time space into six vertical levels (0 m $\leq z <$ 20 m, 20 m $\leq z <$ 40 m, 40 m $\leq z <$ 60 m, 60 m $\leq z <$ 80 m, 80 m $\leq z <$ 105 m, and 105 m $\leq z \leq$ 125 m) and 372 monthly intervals (from January 1989 to December 2019). Then, we bulk-averaged all data points falling in each grid cell of the depth-time space and used the mapped data for further analyses. We did not attempt to interpolate or extrapolate the data to fill in empty grid cells, except the use of 12-month moving averages as shown in Fig. 1A. When we analyzed the data for the entire euphotic zone, we averaged or integrated the mapped data vertically. This gives a total of 277 data points for PO_4 time series and a total of 275 data points for PC:PP ratios with overlapping 269 data points for the scatter plot in Fig. 1 (B and C). When the depths are divided into the upper and lower euphotic zone, we took averages or integrals of the upper three layers (0 m $\leq z <$ 60 m) for the upper euphotic zone and the lower three layers (60 m $\leq z \leq$ 125 m) for the lower euphotic zone. Note that this division is equivalent to the use of a depth criteria of $z <$ 75 m and $z \geq$ 75 m for the upper and lower euphotic zones, respectively, due to the limited sampling depths, enabling us to compare our results with the ones from a previous study (*25*). For sinking PC and PP fluxes, we used the sediment trap–based flux data at 150 m and mapped the data in time by bulk averaging all data points falling into each monthly grid cell.

The method of measuring organic P in both suspended and sinking particles (in particular, ways in which samples are treated) has been modified since November 2011, as detailed in a note of https://hahana.soest.hawaii.edu/hot/hot-dogs/documentation/addendum.html. This modification hampers estimating long-term trends in organic P content and the C:P ratios of suspended and sinking particles at Station ALOHA. Nevertheless, a major fraction of the inverse relationship between the observed C:P ratios and PO_4 concentrations occurs before November 2011 (Fig. 1A and fig. S3). Hence, the methodological shift does not change our conclusion here.

We also present the monthly mean time-series data from the BATS in the North Atlantic Subtropical Gyre at 31°50′N, 63°10′W (*15*) and the spatially distributed climatological mean data for suspended organic matter C:P ratios and PO_4 concentrations. We followed the same procedure, which was applied to the HOT data, to the BATS data to estimate the vertically averaged C:P ratios and PO_4 concentrations within the top 125 m (or the C:P ratios of sinking flux at 150 m). For the BATS data, we used the data for the time period spanning from October 2004 to December 2021 over which the high-precision MAGIC was used to measure PO_4 concentrations (*15*). The spatially distributed C:P data (*32*) shallower than 100 m were mapped into a global ocean domain with a 1° by 1° resolution by bulk-averaging all data points falling into each grid cell. The mapped C:P data are plotted along with the climatological annual-mean PO_4 data (*33*) averaged over 0 to 100 m.

For all the HOT and BATS time series and the spatially distributed data, the C:P ratios were calculated using the depth-averaged PC and PP time series. The statistical analyses of the HOT and BATS time series data were performed using MATLAB, and the confidence levels were determined using the *t* test.

Earth system model

We used the fully coupled CESM2 (*34*) to explore the role of flexible phytoplankton C:P stoichiometry in global ocean NPP and carbon cycles. The model configurations include the atmospheric component of Community Atmosphere Model 6, the land component of Community Land Model version 5, sea ice component (CICE5.1.2), the ocean component from Parallel Ocean Program version 2, and the ocean biogeochemistry component of marine biogeochemistry library (MARBL) fundamentally based on biogeochemistry elemental cycling model (*36*, *39*). The model simulations were carried out for a time period of 1850–2100. These model simulations follow the CMIP6 protocol with historical radiative forcing from 1850 to 2014 and a future projection (SSP3-7.0) from 2015 to 2100 (*35*). We simulated three ensemble members for each C:P assumption starting from different initial conditions differentiated by the maximum (named as 1231.011), minimum (named as 1281.011), and transient (named as 1301.011) states of the Atlantic meridional overturning circulation from the preindustrial spin-up (*35*). Because the differences across different C:P assumptions are substantially larger than the differences across the ensemble members, we mainly present the results from a single ensemble member (1301.011) from each model setup, unless otherwise stated.

The MARBL uses dissolved inorganic carbon, phosphate, nitrate, ammonium, silicate, iron, DOP, and dissolved organic nitrogen as basic currencies for biological production. There are three phytoplankton functional types including small phytoplankton (which represents nano- and picophytoplankton), large phytoplankton (which represents diatoms that build silica frustules), and diazotrophs (which represents the microbes that fix N_2). There is only one zooplankton group and an implicit representation of detritus sinking and remineralization.

The source/sink term for phytoplankton carbon biomass (B_i) is given by

$$J_{Bi} = \mu_i B_i - G(B_i') - m_i T_f B_i' - A(B_i') \quad (1)$$

where μ_i represents the phytoplankton growth rate and i = 1,2,3 represents the three phytoplankton functional types. The sink term "G" represents grazing by zooplankton, "m_i" represents a linear mortality constant, and "A" represents aggregations. The sink terms depend on B'_i, which represents an excess biomass beyond a temperature- and depth-dependent threshold. Both grazing and mortality increase with increasing temperature as formulated as a temperature dependence of $T_f = 1.7^{(T - 30°C)/10°C}$. The first term in the right-hand side $\mu_i B_i$ is the model expression of NPP, which represents the net effect of gross production and respiration by phytoplankton.

The phytoplankton growth rate is computed as the product of resource unlimited growth rate ($\mu_{ref,i}$) at reference temperature (30°C), temperature dependence (T_f), nutrient limitation (V_i), and light availability (L_i) terms as

$$\mu_i = \mu_{ref,i} T_f V_i L_i \quad (2)$$

The nutrient limitation term V_i follows the Liebig's law of the minimum, determined by the most limiting nutrient. The limiting nutrients are N, P, Si, and Fe for large phytoplankton; N, P, and Fe for small phytoplankton; and P and Fe for diazotrophs. Each nutrient limitation factor, indicating nutrient availability relative to nutrient requirement by phytoplankton, is formulated as Michaelis-Menten kinetics with distinct half-saturation constants across different phytoplankton functional types and across different nutrients. With smaller half-saturation constants assigned to small phytoplankton, small phytoplankton outcompete large phytoplankton when nutrients are scarce. Detailed model descriptions and parameter values are presented in a previous study (*36*). Note that the phytoplankton growth rates are not a direct function of our assumed phytoplankton C:P ratios. Instead, phytoplankton growth rates are indirectly influenced by phytoplankton uptake P:C ratios (i.e., the inverse of the C:P ratios; the phytoplankton P uptake per unit C fixation), which can modulate the euphotic zone PO_4 availability and the nutrient limitation term V_i in Eq. 2.

The growth rates of phytoplankton P biomass and phytoplankton P (both PO_4 and DOP) uptake rates are determined by multiplying the phytoplankton carbon biomass growth rates (μ_i) with our assumed P:C stoichiometric ratios. The P:C stoichiometric ratios are parameterized according to empirically determined relationships between suspended particle P:C ratios and ambient PO_4 concentrations or a globally uniform P:C ratio of 1:117 (*40*) (see Sensitivity experiments using an Earth system model) . The use of a globally uniform P:C ratio of 1:106 (*53*) would not make a discernible difference in our conclusions as long as the ratio is spatially and temporally invariant, because we are concerned with how variable or fixed phytoplankton C:P ratios would influence NPP changes from the present to the future. In the variable C:P setups, an upper bound of P:C (or a lower bound of C:P) is set at P:C = 1:117 as provided as a default model setup (*36*). The prescribed upper bound of P:C would not substantially influence our results because, in regions with high surface PO_4 (corresponding to higher phytoplankton P:C ratio regions), phytoplankton growth is typically limited by light or micronutrients. Therefore, changes in surface PO_4 and the P:C uptake ratios would have negligible impacts on simulated NPP in such eutrophic regions.

The model assumes that the same C:P ratios are applied to all phytoplankton functional types at a given PO_4 concentration. Because of this assumption, the global responses of the phytoplankton composition to 21st century climate change are similar across the sensitivity experiments (fig. S9). However, regionally, the relative proportions of NPP by each phytoplankton type are sensitive to the different phytoplankton C:P assumptions, which arises mainly because of competitions between large and small phytoplankton. The diazotrophs contribution to oligotrophic gyre NPP is also slightly modulated by the different C:P assumptions. In our model, diazotrophs fix 25% more N_2 than the cell N quota and excrete the excess N as a bioavailable N such that elemental composition in surface seawater can be modulated by N_2 fixation (*39*). Because of the compensatory effects between flexible C:N (less N uptake when phytoplankton is N-stressed) and N_2 fixation (use

atmospheric N_2 when phytoplankton is N-stressed), our assumption of a fixed phytoplankton C:N ratio can result in the role of diazotrophs in NPP responses being overestimated in this study. However, the uncertainty arising from the fixed C:N assumption is likely to be within the uncertainty of model representations of diazotrophic growth and mortality/grazing. Nonetheless, the phytoplankton type–dependent responses in phytoplankton C:N:P ratios and their contributions to NPP need to be reassessed in future studies with more sophisticated model implementations of phytoplankton C:N:P plasticity supported by observations.

The model assumes that the C:P ratio of phytoplankton directly translates into the C:P ratio of vertically exported POM without preferential remineralization of phytoplankton P. Preferential P remineralization might occur in the real ocean (*15*) and partly explain the elevated POM C:P sensitivity to a decrease in PO_4 as shown in Fig. 1D and fig. S3 (although a greater proportion of inorganic carbon in sinking particles can also elevate the observed C:P ratios in sinking fluxes). In the oligotrophic regions, however, diurnal migration of P-rich zooplankton is known to efficiently export organic P relative to organic C within the upper 500 m (*54*), which might compensate the effect of preferential remineralization of sinking organic phosphorus (*42*). Hence, our assumption of depth-invariant C:P export ratios might be reasonable, given the absence of zooplankton diurnal migration processes in our model. The major sources of POC are production during grazing and via phytoplankton/zooplankton mortality or aggregation of dissolved organic carbon (DOC) (*20*, *39*). The POM remineralization is implicitly parameterized according to (*55*). The total POC flux is the sum of the POC associated with ballast minerals (opal, carbonate minerals, and dust), which is remineralized only when the minerals dissolve, and the excess POC, which is remineralized mostly within the upper water column. The remineralization length scale is depth dependent (without temperature dependence) and increases linearly under low oxygen conditions. The association with ballast minerals enhances the export efficiency.

Dissolved organic matter (DOM) in the MARBL includes semilabile and refractory DOM of carbon, nitrogen, and phosphorus (*56*, *57*). Both semilabile and refractory DOM are produced by the mortality and aggregations of phytoplankton and zooplankton and incomplete phytoplankton consumption by zooplankton. The fractions by which phytoplankton losses and grazing fluxes are allocated to refractory DOM are parameterized with fixed values. The model allocates 6% of POM remineralization flux to the production of refractory DOM. The degradation of DOM by heterotrophic bacteria is parameterized with lifetimes of DOM that are different between DOC and DOP and between semilabile and refractory DOM. The remineralization of DOM is light dependent, with enhanced remineralization of refractory DOM due to photodegradation in the presence of light and the opposing enhanced remineralization of semilabile DOM in the dark. Preferential remineralization of DOP enriches the C:P ratios in DOM pools. Under PO_4-stressed conditions, phytoplankton can consume semilabile DOP (all of which is assumed to be bioavailable) as a P source to balance their nutrient requirements. The global mean elemental composition of total DOM in CESM2 is 385:29:1 (*36*). Further details of DOM parameterization in the MARBL is provided in (*57*) .

Phytoplankton calcification rates vary as a function of small phytoplankton NPP with a fraction depending on the small phytoplankton nutrient limitation term and temperature. Opal production by large phytoplankton is a product of large phytoplankton production and a flexible C:Si elemental ratio, the latter of which is determined by dissolved Fe and Si availability (*36*, *39*). The model also implements a flexible C:Fe elemental ratio of phytoplankton, which is elevated when ambient concentrations of dissolved Fe are low (*36*, *39*).

Decomposition analyses

To understand the mechanisms by which flexible phytoplankton stoichiometric ratios influence ocean NPP, we decomposed the NPP equations, $NPP = \Sigma_{i=1}^{3}(\mu_i \cdot B_i)$ using the first-order approximations of Taylor series expansion. The NPP difference between variable and fixed C:P cases (defined as ΔNPP below) is attributed to differences because of phytoplankton growth rate and because of phytoplankton biomass as

$$\Delta NPP = \Sigma_{i=1}^{3}\Delta NPP_i = \Sigma_{i=1}^{3}(\Delta\mu_i \cdot B_i) + \Sigma_{i=1}^{3}(\mu_i \cdot \Delta B_i) \quad (3)$$

The decomposition results are summarized in fig. S5, which shows that both phytoplankton growth rates and biomass contribute to the estimated NPP differences between the variable and fixed C:P simulations. Figure S5 also shows that the first-order approximation captures the estimated NPP differences well.

The difference in growth rate $\Delta\mu_i$ is further decomposed into the contributions from temperature, nutrients, and light limitation factors as follows

$$\Delta\mu_i = \mu_{ref,i} \cdot \Delta T_f \cdot V_i \cdot L_i + \mu_{ref,i} \cdot T_f \cdot \Delta V_i \cdot L_i + \mu_{ref,i} \cdot T_f \cdot V_i \cdot \Delta L_i \quad (4)$$

The results of the growth rate decomposition analyses are summarized in fig. S6, which shows nearly negligible effects from temperature controlling factor and dominant contributions from nutrient limitation factor. The effects of nutrient availability, favoring greater growth rates under the variable C:P assumption than the fixed C:P assumption, are partly negated by light availability terms that tend to suppress growth rates under the variable C:P assumption due to higher chlorophyll concentrations and light absorption near the sea surface.

CMIP6 data analyses

We explored how nutrient uptake plasticity influences future projections of ocean primary production among the models participating in CMIP6. To this end, we selected 10 Earth system models (tables S1 and S2) and used "historical" and "SSP370" experiments for a single ensemble member of each model. We categorized these Earth system models into two groups based on their representations of phytoplankton nutrient uptake plasticity: (i) models with flexible phytoplankton C:N*:P:Fe ratios where flexible C:N* includes flexible phytoplankton C:N composition or phytoplankton's ability to fix N_2 to meet their N demand, both of which can alleviate N-stress for phytoplankton growth; and (ii) models with nonflexible C:N*:P:Fe, which include all Earth system models that do not allow a full plasticity in C:N*:P:Fe. The models that do not resolve P cycles (e.g., CanESM CanOE, CanESM CMOC, and UKESM MEDUSA) were regarded as having flexible C:P, because P is not limiting phytoplankton growth in the model. Likewise, the models that do not have Fe as a state variable are regarded as having flexible C:Fe as long as Fe limitation is not diagnostically

imposed. For example, CanESM CMOC is categorized as nonflexible C:N*:P:Fe, despite no explicit representations of P and Fe cycling, because the Fe limitation term is diagnosed from the present-day oceanic nitrate distributions (*31*, *58*). We found that only two models (table S1) can be categorized into flexible C:N*:P:Fe (flexible C:N*, flexible C:P, and flexible C:Fe), while the remaining models (table S2) belong to nonflexible C:N*:P:Fe (nonflexible C:N* or nonflexible C:P or nonflexible C:Fe). The two models categorized into flexible C:N*:P:Fe also allow flexible C:Si as well. Therefore, our categorization is equivalently based on whether the models allow full plasticity of all essential nutrients limiting phytoplankton growth. We globally and vertically integrated primary productivity or NPP, whichever is available as model outputs, and plotted them as percentage changes with respect to historical means (1850–2014) as shown in Fig. 2B and fig. S11A. We also globally integrated carbon export production at 100 m and plotted them as percentage changes with respect to historical means (1850–2014) as shown in fig. S11B.

Supplementary Materials

This PDF file includes:

Figs. S1 to S11
Tables S1 and S2
References

REFERENCES AND NOTES

1. R. Geider, J. La Roche, Redfield revisited: Variability of C:N:P in marine microalgae and its biochemical basis. *Eur. J. Phycol.* **37**, 1–17 (2002).
2. J. D. Liefer, A. Garg, M. H. Fyfe, A. J. Irwin, I. Benner, C. M. Brown, M. J. Follows, A. W. Omta, Z. V. Finkel, The macromolecular basis of phytoplankton C:N:P under nitrogen starvation. *Front. Microbiol.* **10**, 763 (2019).
3. R. W. Eppley, B. J. Peterson, Particulate organic matter flux and planktonic new production in the deep ocean. *Nature* **282**, 677–680 (1979).
4. R. F. Heneghan, E. Galbraith, J. L. Blanchard, C. Harrison, N. Barrier, C. Bulman, W. Cheung, M. Coll, T. D. Eddy, M. Erauskin-Extramiana, J. D. Everett, J. A. Fernandes-Salvador, D. Gascuel, J. Guiet, O. Maury, J. Palacios-Abrantes, C. M. Petrik, H. du Pontavice, A. J. Richardson, J. Steenbeek, T. C. Tai, J. Volkholz, P. A. Woodworth-Jefcoats, D. P. Tittensor, Disentangling diverse responses to climate change among global marine ecosystem models. *Prog. in Oceanogr.* **198**, 102659 (2021).
5. S. Bertilsson, O. Berglund, D. M. Karl, S. W. Chisholm, Elemental composition of marine *Prochlorococcus* and *Synechococcus*: Implications for the ecological stoichiometry of the sea. *Limnol. Oceanogr.* **48**, 1721–1731 (2003).
6. A. C. Martiny, C. T. A. Pham, F. W. Primeau, J. A. Vrugt, J. K. Moore, S. A. Levin, M. W. Lomas, Strong latitudinal patterns in the elemental ratios of marine plankton and organic matter. *Nature Geosci.* **6**, 279–283 (2013).
7. C. A. Garcia, S. E. Baer, N. S. Garcia, S. Rauschenberg, B. S. Twining, M. W. Lomas, A. C. Martiny, Nutrient supply controls particulate elemental concentrations and ratios in the low latitude eastern Indian Ocean. *Nat. Commun.* **9**, 4868 (2018).
8. T. Tanioka, K. Matsumoto, A meta-analysis on environmental drivers of marine phytoplankton C:N:P. *Biogeosciences* **17**, 2939–2954 (2020).
9. E. D. Galbraith, A. C. Martiny, A simple nutrient-dependence mechanism for predicting the stoichiometry of marine ecosystems. *Proc. Natl. Acad. Sci. U.S.A.* **112**, 8199–8204 (2015).
10. W. F. Cross, J. M. Hood, J. P. Benstead, A. D. Huryn, D. Nelson, Interactions between temperature and nutrients across levels of ecological organization. *Glob. Change Biol.* **21**, 1025–1040 (2014).
11. B. A. S. Van Mooy, H. F. Fredricks, B. E. Pedler, S. T. Dyhrman, D. M. Karl, M. Koblízek, M. W. Lomas, T. J. Mincer, L. R. Moore, T. Moutin, M. S. Rappé, E. A. Webb, Phytoplankton in the ocean use non-phosphorus lipids in response to phosphorus scarcity. *Nature* **458**, 69–72 (2009).
12. A. Toseland, S. J. Daines, J. R. Clark, A. Kirkham, J. Strauss, C. Uhlig, T. M. Lenton, K. Valentin, G. A. Pearson, V. Moulton, T. Mock, The impact of temperature on marine phytoplankton resource allocation and metabolism. *Nat. Clim. Change* **3**, 979–984 (2013).
13. A. C. Martiny, G. I. Hagstrom, T. De Vries, R. T. Letscher, G. L. Britten, C. A. Garcia, E. Galbraith, D. Karl, S. A. Levin, M. W. Lomas, A. R. Moreno, D. Talmy, W. Wang, K. Matsumoto, Marine phytoplankton resilience may moderate oligotrophic ecosystem responses and biogeochemical feedbacks to climate change. *Limnol. Oceanogr.* **67**, S378–S389 (2022).
14. A. Quigg, Z. V. Finkel, A. J. Irwin, Y. Rosenthal, T.-Y. Ho, J. R. Reinfelder, O. Schofield, F. M. M. Morel, P. G. Falkowski, The evolutionary inheritance of elemental stoichiometry in marine phytoplankton. *Nature* **425**, 291–294 (2003).
15. M. W. Lomas, N. R. Bates, R. J. Johnson, D. K. Steinberg, T. Tanioka, Adaptive carbon export response to warming in the Sargasso Sea. *Nat. Commun.* **13**, 1211 (2022).
16. T. Tanioka, C. Garcia, A. Larkin, N. Garcia, A. Fagan, A. Martiny, Global patterns and drivers of C:N:P in marine ecosystems. *Commun. Earth Environ.* **3**, 271 (2022).
17. L. Kwiatkowski, O. Aumont, L. Bopp, P. Ciais, The impact of variable phytoplankton stoichiometry on projections of primary production, food quality, and carbon uptake in the global ocean. *Global Bigeochem. Cycles* **32**, 516–528 (2018).
18. T. Tanioka, K. Matsumoto, Buffering of ocean export production by flexible elemental stoichiometry of particulate organic matter. *Global Bigeochem. Cycles* **31**, 1528–1542 (2017).
19. L. Bopp, L. Resplandy, J. C. Orr, S. C. Doney, J. P. Dunne, M. Gehlen, P. Halloran, C. Heinze, T. Ilyina, R. Séférian, J. Tjiputra, M. Vichi, Multiple stressors of ocean ecosystems in the 21st century: Projections with CMIP5 models. *Biogeosciences* **10**, 6225–6245 (2013).
20. C. Laufkötter, M. Vogt, N. Gruber, M. Aita-Noguchi, O. Aumont, L. Bopp, E. Buitenhuis, S. C. Doney, J. Dunne, T. Hashioka, J. Hauck, T. Hirata, J. John, C. le Quéré, I. D. Lima, H. Nakano, R. Seferian, I. Totterdell, M. Vichi, C. Völker, Drivers and uncertainties of future global marine primary production in marine ecosystem models. *Biogeosciences* **12**, 6955–6984 (2015).
21. J. K. Moore, W. Fu, F. Primeau, G. L. Britten, K. Lindsay, M. Long, S. C. Doney, N. Mahowald, F. Hoffman, J. T. Randerson, Sustained climate warming drives declining marine biological productivity. *Science* **359**, 1139–1143 (2018).
22. M. J. Behrenfeld, R. T. O'Malley, D. A. Siegel, C. R. McClain, J. L. Sarmiento, G. C. Feldman, A. J. Milligan, P. G. Falkowski, R. M. Letelier, E. S. Boss, Climate-driven trends in contemporary ocean productivity. *Nature* **444**, 752–755 (2006).
23. R. Yamaguchi, T. Suga, Trend and variability in global upper-ocean stratification since the 1960s. *J. Geophys. Res.: Oceans* **124**, 8933–8948 (2019).
24. W. W. Gregg, C. S. Rousseaux, Global ocean primary production trends in the modern ocean color satellite record (1998–2015). *Environ. Res. Lett.* **14**, 124011 (2019).
25. D. M. Karl, R. M. Letelier, R. R. Bidigare, K. M. Björkman, M. J. Church, J. E. Dore, A. E. White, Seasonal-to-decadal scale variability in primary production and particulate matter export at Station ALOHA. *Progr. Oceanogr.* **195**, 102563 (2021).
26. R. M. Letelier, K. M. Björkman, M. J. Church, D. S. Hamilton, N. M. Mahowald, R. A. Scanza, N. Schneider, A. E. White, D. M. Karl, Climate-driven oscillation of phosphorus and iron limitation in the North Pacific Subtropical Gyre. *Proc. Natl. Acad. Sci. U.S.A.* **116**, 12720–12728 (2019).
27. A. C. Martiny, M. W. Lomas, W. Fu, P. W. Boyd, Y. L. L. Chen, G. A. Cutter, M. J. Ellwood, K. Furuya, F. Hashihama, J. Kanda, D. M. Karl, T. Kodama, Q. P. Li, J. Ma, T. Moutin, E. M. S. Woodward, J. K. Moore, Biogeochemical controls of surface ocean phosphate. *Sci. Adv.* **5**, eaax0341 (2019).
28. L. Kwiatkowski, O. Torres, L. Bopp, O. Aumont, M. Chamberlain, J. R. Christian, J. P. Dunne, M. Gehlen, T. Ilyina, J. G. John, A. Lenton, H. Li, N. S. Lovenduski, J. C. Orr, J. Palmieri, Y. Santana-Falcón, J. Schwinger, R. Séférian, C. A. Stock, A. Tagliabue, Y. Takano, J. Tjiputra, K. Toyama, H. Tsujino, M. Watanabe, A. Yamamoto, A. Yool, T. Ziehn, Twenty-first century ocean warming, acidification, deoxygenation, and upper-ocean nutrient and primary production decline from CMIP6 model projections. *Biogeosciences* **17**, 3439–3470 (2020).
29. R. Séférian, S. Berthet, A. Yool, J. Palmiéri, L. Bopp, A. Tagliabue, L. Kwiatkowski, O. Aumont, J. Christian, J. Dunne, M. Gehlen, T. Ilyina, J. G. John, H. Li, M. C. Long, J. Y. Luo, H. Nakano, A. Romanou, J. Schwinger, C. Stock, Y. Santana-Falcón, Y. Takano, J. Tjiputra, H. Tsujino, M. Watanabe, T. Wu, F. Wu, A. Yamamoto, Tracking improvement in simulated marine biogeochemistry between CMIP5 and CMIP6. *Curr. Clim. Change Rep.* **6**, 95–119 (2020).
30. L. Bopp, O. Aumont, L. Kwiatkowski, C. Clerc, L. Dupont, C. Ethé, T. Gorgues, R. Séférian, A. Tagliabue, Diazotrophy as a key driver of the response of marine net primary productivity to climate change. *Biogeosciences* **19**, 4267–4285 (2022).
31. J. R. Christian, K. L. Denman, H. Hayashida, A. M. Holdsworth, W. G. Lee, O. G. J. Riche, A. E. Shao, N. Steiner, N. C. Swart, Ocean biogeochemistry in the Canadian Earth System Model version 5.0.3: CanESM5 and CanESM5-CanOE. *Geosci. Model Dev.* **15**, 4393–4424 (2022).
32. A. C. Martiny, J. A. Vrugt, M. W. Lomas, Concentrations and ratios of particulate organic carbon, nitrogen, and phosphorus in the global ocean. *Sci. Data* **1**, 140048 (2014).
33. H. E. Garcia, K. W. Weathers , C. R. Paver, I. Smolyar , T. P. Boyer, M. M. Locarnini, M. M. Zweng, A. V. Mishonov , O. K. Baranova, D. Seidov, J. R. Reagan, "World Ocean Atlas 2018, Volume 4:

Dissolved inorganic nutrients (phosphate, nitrate and nitrate+nitrite, silicate)," (NOAA Atlas NESDIS, 2018).
34. G. Danabasoglu, J.-F. Lamarque, J. Bacmeister, D. A. Bailey, A. K. Du Vivier, J. Edwards, L. K. Emmons, J. Fasullo, R. Garcia, A. Gettelman, C. Hannay, M. M. Holland, W. G. Large, P. H. Lauritzen, D. M. Lawrence, J. T. M. Lenaerts, K. Lindsay, W. H. Lipscomb, M. J. Mills, R. Neale, K. W. Oleson, B. Otto-Bliesner, A. S. Phillips, W. Sacks, S. Tilmes, L. van Kampenhout, M. Vertenstein, A. Bertini, J. Dennis, C. Deser, C. Fischer, B. Fox-Kemper, J. E. Kay, D. Kinnison, P. J. Kushner, V. E. Larson, M. C. Long, S. Mickelson, J. K. Moore, E. Nienhouse, L. Polvani, P. J. Rasch, W. G. Strand, The Community Earth System Model version 2 (CESM2). *J. Adv. Mod. Earth Syst.* **12**, e2019MS001916 (2020).
35. K. B. Rodgers, S.-S. Lee, N. Rosenbloom, A. Timmermann, G. Danabasoglu, C. Deser, J. Edwards, J.-E. Kim, I. R. Simpson, K. Stein, M. F. Stuecker, R. Yamaguchi, T. Bódai, E. S. Chung, L. Huang, W. M. Kim, J.-F. Lamarque, D. L. Lombardozzi, W. R. Wieder, S. G. Yeager, Ubiquity of human-induced changes in climate variability. *Earth Syst. Dynam.* **12**, 1393–1411 (2021).
36. M. C. Long, J. K. Moore, K. Lindsay, M. Levy, S. C. Doney, J. Y. Luo, K. M. Krumhardt, R. T. Letscher, M. Grover, Z. T. Sylvester, Simulations with the marine biogeochemistry library (MARBL). *J. Adv. Model. Earth Syst.* **13**, e2021MS002647 (2021).
37. W.-L. Wang, J. K. Moore, A. C. Martiny, F. W. Primeau, Convergent estimates of marine nitrogen fixation. *Nature* **566**, 205–211 (2019).
38. J. K. Moore, S. C. Doney, J. A. Kleypas, D. M. Glover, I. Y. Fung, An intermediate complexity marine ecosystem model for the global domain. *Deep-Sea Res. II Top. Stud. Oceanogr.* **49**, 403–462 (2001).
39. J. K. Moore, S. C. Doney, K. Lindsay, Upper ocean ecosystem dynamics and iron cycling in a global three-dimensional model. *Global Bigeochem. Cycles* **18**, (2004).
40. L. A. Anderson, J. L. Sarmiento, Redfield ratios of remineralization determined by nutrient data analysis. *Global Bigeochem. Cycles* **8**, 65–80 (1994).
41. A. R. Moreno, G. I. Hagstrom, F. W. Primeau, S. A. Levin, A. C. Martiny, Marine phytoplankton stoichiometry mediates nonlinear interactions between nutrient supply, temperature, and atmospheric CO_2. *Biogeosciences* **15**, 2761–2779 (2018).
42. E. Y. Kwon, M. Holzer, A. Timmermann, F. Primeau, Estimating three-dimensional Carbon-To-Phosphorus stoichiometry of exported marine organic matter. *Global Bigeochem. Cycles* **36**, e2021GB007154 (2022).
43. A. Tagliabue, L. Kwiatkowski, L. Bopp, M. Butenschön, W. Cheung, M. Lengaigne, J. Vialard, Persistent uncertainties in ocean net primary production climate change projections at regional scales raise challenges for assessing impacts on ecosystem services. *Front. Clim.* **3**, 16 (2021).
44. T. Tyrrell, The relative influences of nitrogen and phosphorus on oceanic primary production. *Nature* **400**, 525–531 (1999).
45. D. M. Karl, R. M. Letelier, Nitrogen fixation-enhanced carbon sequestration in low nitrate, low chlorophyll seascapes. *Mar. Ecol. Prog. Ser.* **364**, 257–268 (2008).
46. D. M. Karl, R. M. Letelier, D. V. Hebel, D. F. Bird, C. D. Winn, *Trichodesmium Blooms and New Nitrogen in the North Pacific Gyre in Marine Pelagic Cyanobacteria: Trichodesmium and Other Diazotrphs* (Klaer Academic Publishers, 1992).
47. C. R. Schvarcz, S. T. Wilson, M. Caffin, R. Stancheva, Q. Li, K. A. Turk-Kubo, A. E. White, D. M. Karl, J. P. Zehr, G. F. Steward, Overlooked and widespread pennate diatom-diazotroph symbioses in the sea. *Nat. Commun.* **13**, 799 (2022).
48. N. J. Hawco, B. Barone, M. J. Church, L. Babcock-Adams, D. J. Repeta, E. K. Wear, R. K. Foreman, K. M. Björkman, S. Bent, B. A. S. van Mooy, U. Sheyn, E. F. DeLong, M. Acker, R. L. Kelly, A. Nelson, J. Ranieri, T. M. Clemente, D. M. Karl, S. G. John, Iron depletion in the deep chlorophyll maximum: Mesoscale eddies as natural iron fertilization experiments. *Global Bigeochem. Cycles* **35**, e2021GB007112 (2021).
49. J. Diaz, E. Ingall, C. Benitez-Nelson, D. Paterson, M. D. de Jonge, I. McNulty, J. A. Brandes, Marine polyphosphate: A key player in geologic phosphorus sequestration. *Science* **320**, 652–655 (2008).
50. D. M. Karl, K. M. Björkman, M. J. Church, L. A. Fujieki, E. M. Grabowski, R. M. Letelier, Temporal dynamics of total microbial biomass and particulate detritus at Station ALOHA. *Progr. Oceanogr.* **205**, 102803 (2022).
51. A. L. Pasulka, M. R. Landry, D. A. A. Taniguchi, A. G. Taylor, M. J. Church, Temporal dynamics of phytoplankton and heterotrophic protists at station ALOHA. *Deep-Sea Res. II Top. Stud. Oceanogr.* **93**, 44–57 (2013).
52. D. M. Karl, R. Lukas, The Hawaii Ocean Time-series (HOT) program: Background, rationale and field implementation. *Deep-Sea Res. II Top. Stud. Oceanogr.* **43**, 129–156 (1996).
53. A. C. Redfield, The biological control of chemical factors in the environment. *Am. Sci.* **46**, 205–221 (1958).
54. C. C. S. Hannides, M. R. Landry, C. R. Benitez-Nelson, R. M. Styles, J. P. Montoya, D. M. Karl, Export stoichiometry and migrant-mediated flux of phosphorus in the North Pacific Subtropical Gyre. *Deep-Sea Res. I Oceanogr. Res. Pap.* **56**, 73–88 (2009).
55. R. A. Armstrong, C. Lee, J. I. Hedges, S. Honjo, S. G. Wakeham, A new, mechanistic model for organic carbon fluxes in the ocean based on the quantitative association of POC with ballast minerals. *Deep-Sea Res. II Top. Stud. Oceanogr.* **49**, 219–236 (2001).
56. R. T. Letscher, J. K. Moore, Preferential remineralization of dissolved organic phosphorus and non-Redfield DOM dynamics in the global ocean: Impacts on marine productivity, nitrogen fixation, and carbon export. *Global Bigeochem. Cycles* **29**, 325–340 (2015).
57. R. T. Letscher, J. K. Moore, Y.-C. Teng, F. Primeau, Variable C:N:P stoichiometry of dissolved organic matter cycling in the Community Earth System Model. *Biogeosciences* **12**, 209–221 (2015).
58. K. Zahariev, J. R. Christian, K. L. Denman, Preindustrial, historical, and fertilization simulations using a global ocean carbon model with new parameterizations of iron limitation, calcification, and N_2 fixation. *Progr. Oceanogr.* **77**, 56–82 (2008).
59. R. J. Geider, H. MacIntyre, T. M. Kana, A dynamic regulatory model of phytoplanktonic acclimation to light, nutrients, and temperature. *Limnol. Oceanogr.* **43**, 679–694 (1998).
60. T. Hajima, M. Watanabe, A. Yamamoto, H. Tatebe, M. A. Noguchi, M. Abe, R. Ohgaito, A. Ito, D. Yamazaki, H. Okajima, A. Ito, K. Takata, K. Ogochi, S. Watanabe, M. Kawamiya, Development of the MIROC-ES2L Earth system model and the evaluation of biogeochemical processes and feedbacks. *Geosci. Model Dev.* **13**, 2197–2244 (2020).
61. H. Paulsen, T. Ilyina, K. D. Six, I. Stemmler, Incorporating a prognostic representation of marine nitrogen fixers into the global ocean biogeochemical model HAMOCC. *J. Adv. Model. Earth Syst.* **9**, 438–464 (2017).
62. C. A. Stock, J. P. Dunne, S. Fan, P. Ginoux, J. John, J. P. Krasting, C. Laufkötter, F. Paulot, N. Zadeh, Ocean biogeochemistry in GFDL's Earth System Model 4.1 and its response to increasing atmospheric CO_2. *J. Adv. Model. Earth Syst.* **12**, e2019MS002043 (2020).
63. O. Aumont, C. Ethé, A. Tagliabue, L. Bopp, M. Gehlen, PISCES-v2: An ocean biogeochemical model for carbon and ecosystem studies. *Geosci. Model Dev.* **8**, 2465–2513 (2015).
64. A. Yool, E. E. Popova, T. R. Anderson, MEDUSA-2.0: An intermediate complexity biogeochemical model of the marine carbon cycle for climate change and ocean acidification studies. *Geosci. Model Dev.* **6**, 1767–1811 (2013).
65. J. F. Tjiputra, J. Schwinger, M. Bentsen, A. L. Morée, S. Gao, I. Bethke, C. Heinze, N. Goris, A. Gupta, Y.-C. He, D. Olivié, Ø. Seland, M. Schulz, Ocean biogeochemistry in the Norwegian Earth System Model version 2 (NorESM2). *Geosci. Model Dev.* **13**, 2393–2431 (2020).

Acknowledgments: We thank scientists who have been involved in development of CESM and MARBL. We also thank scientists who have contributed to the HOT and BATS databases. We are grateful for continuous discussions with K. Rodgers and a discussion with D. Bianchi, which have helped us improve this manuscript. The CESM2 simulations were conducted on the ICCP/IBS supercomputer Aleph, a Cray XC50-LC system. **Funding:** This study is supported by Institute for Basic Science (IBS-R028-D1). E.Y.K. also acknowledges funding from Korean National Research Foundation (NRF-2016R1D1A1B04931356). D.M.K. acknowledges funding from Simons Foundation (#721252) and National Science Foundation (NSF-OCE-1756517). M.J.C. acknowledges funding from Simons Foundation (#721221). **Author contributions:** E.Y.K. and A.T. designed this study. M.G.S. and S.-S.L. performed CESM2 experiments. M.G.S. and E.Y.K. analyzed the model results with inputs from A.T. and R.Y. E.Y.K. analyzed the time-series data and the spatially averaged climatological mean data with inputs from D.M.K. and M.J.C. E.Y.K. and M.G.S. wrote and reviewed the manuscript with inputs from A.T., D.M.K., M.J.C., R.Y., and S.-S.L. **Competing interests:** The authors declare that they have no competing interests. **Data and materials availability:** All data needed to evaluate the conclusions in the paper are present in the paper and/or the Supplementary Materials. The HOT data are available at https://hahana.soest.hawaii.edu/hot/hot-dogs/interface.html. The BATS data are available at http://bats.bios.edu/bats-data/. The CESM2 simulations with variable C:P (a hyperbolic relationship between phytoplankton C:P and phosphate concentration) are available at www.cesm.ucar.edu/projects/community-projects/LENS2/data-sets.html. The other CESM2 simulations with variable C:P (a power-law relationship between phytoplankton C:P and phosphate concentration) and fixed C:P are available at the OPeNDAP server https://climatedata.ibs.re.kr/data/cesm2-senctop. The CMIP6 model outputs are available at https://esgf-node.llnl.gov/search/cmip6/. The CESM code is available at www.cesm.ucar.edu/models/cesm2/release_download.html.

Submitted 30 May 2022
Accepted 18 November 2022
Published 21 December 2022
10.1126/sciadv.add2475